Lithium Storage in Nanostructured TiO_2 Made by Hydrothermal Growth

Ladislav Kavan,*[,†,⊥] Martin Kalbáč,[†] Markéta Zukalová,[†] Ivan Exnar,[‡] Volker Lorenzen,[§] Reinhard Nesper,[∥] and Michael Graetzel[⊥]

J. Heyrovský Institute of Physical Chemistry, Academy of Sciences of the Czech Republic, Dolejškova 3, CZ-18223 Prague 8, Czech Republic, High Power Lithium, Park Scientifique, PSE-B, EPFL, Ecublens, CH-1015 Lausanne, Switzerland, SusTech GmbH & Co. KG, Petersenstr. 20, D-64287 Darmstadt, Germany, Laboratory of Inorganic Chemistry, ETHZ, Wolfgang-Pauli-Str. 10, CH-8093 Zürich, Switzerland, and Laboratory of Photonics and Interfaces, EPFL, Ecublens, CH-1015 Lausanne, Switzerland

Received October 21, 2003. Revised Manuscript Received November 24, 2003

Nanostructured titania materials were prepared from $TiCl_4$ via autoclaving in 10 M NaOH at 250 °C and subsequent treatment in aqueous and/or acidic media. XRD and Raman spectroscopy evidenced the presence of anatase as the main phase, but most materials contained also some XRD-silent component. Cyclic voltammograms of lithium insertion demonstrate two pairs of reversible pseudocapacitive peaks (S-peaks) in addition to the ordinary peaks of diffusion-controlled Li insertion into the anatase lattice. The occurrence of S-peaks is associated with the nanosheet- and/or nanotubular morphology of the materials. This structure developed at hydrothermal conditions via exfoliation of the layered Na^+/H^+ titanate precursors. The S-peaks were suggested to be the signatures of quantum-size confinement in titania nanosheets. The nanosheet-containing materials are reducible by *n*-butyllithium to cubic $LiTiO_2$ (at conditions when the ordinary nanocrystalline anatase gives only the orthorhombic $Li_{0.5}TiO_2$). Consequently, the electrochemical Li-storage capacity is larger compared to that of crystalline anatase. The prepared materials also show better insertion kinetics; hence, they are promising for applications in Li-ion batteries. Depending on the applied voltage, they can be charged/discharged either as ordinary Li-insertion hosts or as supercapacitors.

Introduction

The insertion/extraction of Li to/from the TiO_2 lattice is described by the equation

$$TiO_2 + x(Li^+ + e^-) \rightarrow Li_xTiO_2 \qquad (1)$$

The most active form of TiO_2 for reaction 1 is anatase, in which the insertion coefficient x is usually close to 0.5.[1−4] Various theoretical[5−7] and experimental[1,3−5,8−14] aspects of reaction 1 have been addressed in the past. Investigations of X-ray diffraction,[13,15] electrical and optical properties,[14] photoelectron spectroscopy,[16] X-ray absorption,[17] and ^{7}Li NMR[15,17−19] unanimously show that anatase converts during reaction 1 into a two-phase product, viz. lithium-poor tetragonal phase $Li_{0.01}TiO_2$ with the anatase structure (space group $I4_1/amd$) and orthorhombic lithium titanate, $Li_{0.5}TiO_2$ (space group $Imma$).

Investigations of single-crystal[8,9] and polycrystalline[3] electrodes have shown that the insertion capacity,

* Corresponding author. E-mail: kavan@jh-inst.cas.cz.
† Academy of Sciences of the Czech Republic.
‡ High Power Lithium, Park Scientifique, PSE-B, EPFL.
§ SusTech GmbH & Co. KG.
∥ ETHZ.
⊥ Laboratory of Photonics and Interfaces, EPFL.

(1) Lindström, H.; Södergen, S.; Solbrand, A.; Rensmo, H.; Hjelm, J.; Hagfeldt, A.; Lindquist, S. E. *J. Phys. Chem. B* **1997**, *101*, 7717−7722.
(2) Kavan, L.; Kratochvilová, K.; Grätzel, M. *J. Electroanal. Chem.* **1995**, *394*, 93−102.
(3) Kavan, L.; Grätzel, M.; Rathousky, J.; Zukal, A. *J. Electrochem. Soc.* **1996**, *143*, 394−400.
(4) Kavan, L.; Attia, A.; Lenzmann, F.; Elder, S. H.; Grätzel, M. *J. Electrochem. Soc.* **2000**, *147*, 2897−2902.
(5) Lunell, S.; Stashans, A.; Lindström, H.; Hagfeldt, A. *J. Am. Chem. Soc.* **1997**, *119*, 7374−7380.
(6) Mackrodt, W. C. *J. Solid State Chem.* **1999**, *142*, 428−439.
(7) Nuspl, G.; Yoshizawa, K.; Yamabe, T. *J. Mater. Chem.* **1997**, *7*, 2529−2536.
(8) Hengerer, R.; Kavan, L.; Krtil, P.; Grätzel, M. *J. Electrochem. Soc.* **2000**, *147*, 1467−1472.
(9) Kavan, L.; Grätzel, M.; Gilbert, S. E.; Klemenz, C.; Scheel, H. J. *J. Am. Chem. Soc.* **1996**, *118*, 6716−6723.
(10) Huang, S. Y.; Kavan, L.; Grätzel, M.; Exnar, I. *J. Electrochem. Soc.* **1995**, *142*, 142−144.
(11) Lindström, H.; Södergen, S.; Solbrand, A.; Rensmo, H.; Hjelm, J.; Hagfeldt, A.; Lindquist, S. E. *J. Phys. Chem. B* **1997**, *101*, 7710−7716.
(12) Van de Krol, R.; Goossens, A.; Schoonman, J. *J. Phys. Chem. B* **1999**, *103*, 7151−7159.
(13) Van de Krol, R.; Goossens, A.; Meulenkamp, E. A. *J. Electrochem. Soc.* **1999**, *146*, 3150−3154.
(14) Van de Krol, R.; Goossens, A.; Meulenkamp, E. A. *J. Appl. Phys.* **2001**, *90*, 2235−2242.
(15) Wagemaker, M.; Van de Krol, R.; Kentgens, A. P. M.; Van Well, A. A.; Mulder, F. M. *J. Am. Chem. Soc.* **2001**, *123*, 11454−11461.
(16) Henningsson, A.; Andersson, M. P.; Uvdal, P.; Siegbahn, H.; Sandell, A. *Chem. Phys. Lett.* **2002**, *360*, 85−90.
(17) Luca, V.; Hanley, T. L.; Roberts, N. K.; Howe, R. F. *Chem. Mater.* **1999**, *11*, 2089−2102.
(18) Wagemaker, M.; Kentgens, A. P. M.; Mulder, F. M. *Nature* **2002**, *418*, 397−399.
(19) Wagemaker, M.; Kearley, G. J.; Van Well, A. A.; Mutka, H.; Mulder, F. M. *J. Am. Chem. Soc.* **2003**, *125*, 840−848.

10.1021/cm035046g CCC: $27.50
Published on Web 01/10/2004

coulombic efficiency, reversibility, and stability of anatase depend on the electrode morphology. However, previous reports have mostly dealt with statistically packed nanocrystals without deliberately controlled particle structure and mesoscopic ordering.[1,3,5,10−13] Li insertion into organized, Pluronic-templated anatase exhibited some abnormal features, which were tentatively assigned to the presence of amorphous titania in the highly organized skeleton.[20]

The preparation of nanostructured anatase in the form of fibers, nanotubes, nanoribbons, and nanowires was attempted by templating with anodic alumina,[21−26] polymers,[27] and low-molecular-weight surfactants.[28−31] Of particular interest is a simple method based on hydrothermal recrystallization in aqueous NaOH pioneered by Kasuga et al.[32] There are also several reports on single-crystalline nanowires[21,26,33] and nanotubes.[31,34] Nevertheless, a perfect single-crystal-like structure, which would be analogous to a carbon nanotube, does not seem to be accessible with anatase. (Note that one claim for the anatase analogue of carbon nanotube[34] was later canceled).

The mechanism of alkaline hydrothermal conversion of titania into nanofibers (tubes, ribbons) was discussed by several authors,[32,35−41] but the results have often been contradictory. Most works have dealt with NaOH medium, but there were also occasional studies in KOH.[35,37] Important intermediates are layered alkali titanates, of the general formula $M_2Ti_nO_{2n+1}$ ($M = Na$, K, $3 \le n \le 6$). They have a monoclinic lattice, with parallel kinked layers of edge-sharing TiO_6 octahedra. Such layers intercalate alkali metal cations M^+, which can be further ion-exchanged with H^+ or H_3O^+ toward protonic hydrous titanates $H_2Ti_nO_{2n+1}\cdot mH_2O$. The reaction is topotactic; hence, the protonic titanates preserve the original layered structure.[42,43] An alternative of this material is orthorhombic $H_xTi_{2-x/4}\square_{x/4}O_4\cdot H_2O$ ($x \approx 0.7$, $\square$ = vacancy) with the lepidocrocite-type structure. It is characterized by stacked flat sheets of edge-sharing TiO_6 octahedra with intercalated H_2O and H_3O^+ (hydroxonium ions are balanced with titanium ion vacancies).[44−46] These layered crystals easily exfoliate into individual nanosheets, exhibiting high two-dimensional anisotropy: thickness of ca. 1 nm and lateral dimension of 0.1−1 μm.[44−46]

The layered protonic titanates seem to be the key structures in the synthesis of nanotextured materials via the alkaline hydrothermal treatment of TiO_2. They are, presumably, produced by the Na^+/H^+ ion exchange during subsequent acidic washing of the alkali autoclaved titania, but some authors have assumed that the protonic titanates grow also directly during the NaOH treatment.[35,36] The morphology has been characterized as nanotube,[32,35,36,38,39,41] fiber,[47] nanowire,[33,37] and nanoribbon.[40] The most typical structure is derived from exfoliated titanate nanosheets which may be rolled into a multiwalled nanotube with spiral cross section.[35,36,39] However, intermediate structures of flat or occasionally curved sheets[35,39−41] are also abundant in the product. (Since the titania nanotubes grow via rolling of the sheet precursors, they do not possess the closed cagelike structure like carbon nanotubes.)

The crystallographic description of these tubular/sheet materials is based on monoclinic protonic titanates[47] such as $H_2Ti_3O_7$,[35,36,41] but other authors considered also the anatase lattice[38,39,40,48] to be the basic structural motif of these sheets/tubes. This was supported by the TEM patterns showing fringes of 0.37 nm (a_0 lattice parameter of anatase) and 0.75−0.78 nm.[39,40] According to this model, the sheets grow along the (001) plane,[39,40] but sheets with denser stacking corresponding to the (101) planes can also be considered.[40] The anatase structure of sheets was also found in the lepidocrocite-like material after mild calcination.[44] Generally, the primary product of alkaline hydrothermal treatment of titania is the Na^+/H^+ titanate, which is free from any crystalline TiO_2 (anatase, rutile, etc.).[36,41] However, thermal dehydratation of protonic titanates leads to TiO_2 (presumably nonstoichiometric), while the anatase and rutile phases grow depending on the pretreatment conditions and the final calcination temperature.[35,36,38,41,42,44,47] Sometimes also TiO_2(B)[42,49] and "monoclinic" TiO_2[47] were identified as intermediate phases during heat treatment. (Note that the "mono-

(20) Kavan, L.; Rathousky, J.; Grätzel, M.; Shklover, V.; Zukal, A. *J. Phys. Chem. B* **2000**, *104*, 12012−12020.
(21) Zhang, X.; Yao, B.; Zhao, L.; Liang, C.; Zhang, L.; Mao, Y. *J. Electrochem. Soc.* **2001**, *148*, G398−G400.
(22) Lin, Y.; Wu, G. S.; Yuan, X. Y.; Xie, T.; Zhang, L. D. *J. Phys. Condens. Matter* **2003**, *15*, 2917−2922.
(23) Zhang, M.; Bando, Y.; Wada, K. *J. Mater. Sci. Lett.* **2001**, *20*, 167−170.
(24) Lei, Y.; Zhang, L. D.; Fan, J. C. *Chem. Phys. Lett.* **2001**, *338*, 231−236.
(25) Hoyer, P. *Langmuir* **1996**, *12*, 1411−1413.
(26) Miao, Z.; Xu, D.; Ouyang, J.; Guo, G.; Zhao, X.; Tang, Y. *Nano Lett.* **2002**, *2*, 717−720.
(27) Caruso, R. A.; Schattka, J. H.; Greiner, A. *Adv. Mater.* **2001**, *13*, 1577−1579.
(28) Kobayashi, S.; Hanabusa, K.; Hamaski, N.; Kimura, M.; Shirai, H. *Chem. Mater.* **2000**, *12*, 1523−1525.
(29) Jung, J. H.; Kobayashi, H.; van Bommel, K. J. C.; Shinkai, S.; Shimizu, T. *Chem. Mater.* **2002**, *14*, 1445−1447.
(30) Adachi, M.; Murata, Y.; Harada, M.; Yoshikawa, S. *Chem. Lett.* **2000**, 942−943.
(31) Adachi, M.; Murata, Y.; Okada, I.; Zaban, A.; Yoshikawa, S. *J. Electrochem. Soc.* **2003**, *150*, G488−G493.
(32) Kasuga, T.; Hiramatsu, M.; Hoson, A.; Sekino, T.; Niihara, K. *Langmuir* **1998**, *14*, 3160−3163.
(33) Xu, C.; Zhan, Y.; Hong, K.; Wang, G. *Solid State Commun.* **2003**, *126*, 545−549.
(34) Liu, S. M.; Gan, L. M.; Liu, L. H.; Zhang, W. D.; Zeng, H. C. *Chem. Mater.* **2002**, *14*, 1391−1397.
(35) Chen, Q.; Zhou, W.; Du, G.; Peng, L. M. *Adv. Mater.* **2002**, *14*, 1208−1211.
(36) Du, G. H.; Chen, Q.; Che, R. C.; Yuan, Z. Y.; Peng, L. M. *Appl. Phys. Lett.* **2001**, *79*, 3702−3704.
(37) Du, G. H.; Chen, Q.; Han, P. D.; Yu, Y.; Peng, L. M. *Phys. Rev. B* **2003**, *67*, 035323−0353237.
(38) Seo, D. S.; Lee, J. K.; Kim, H. *J. Cryst. Growth* **2001**, *229*, 428−432.
(39) Yao, B. D.; Chan, Y. F.; Zhang, X. Y.; Zhang, W. F.; Yang, Z. Y.; Wang, N. *Appl. Phys. Lett.* **2003**, *82*, 281−283.
(40) Yuan, Z. Y.; Colomer, J. F.; Su, B. L. *Chem. Phys. Lett.* **2002**, *363*, 362−366.
(41) Sun, X.; Li, Y. *Chem. Eur. J.* **2003**, *9*, 2229−2238.
(42) Sasaki, T.; Komatsu, Y.; Fujiki, Y. *Chem. Mater.* **1992**, *4*, 894−899.
(43) Sasaki, T.; Watanabe, M.; Komatsu, Y.; Fujiki, Y. *Inorg. Chem.* **1985**, *24*, 2265−2271.
(44) Sasaki, T.; Nakano, S.; Yamauchi, S.; Watanabe, M. *Chem. Mater.* **1997**, *9*, 602−608.
(45) Sasaki, T.; Watanabe, M. *J. Am. Chem. Soc.* **1998**, *120*, 4682−4689.
(46) Choy, J. H.; Lee, H. C.; Jung, H.; Kim, H.; Boo, H. *Chem. Mater.* **2002**, *14*, 2486−2491.
(47) Yin, S.; Fujishiro, Y.; Wu, J.; Aki, M.; Sato, T. *J. Mater. Proc. Technol.* **2003**, *137*, 45−48.
(48) Zhou, Y.; Cao, L.; Zhang, F.; He, B.; Li, H. *J. Electrochem. Soc.* **2003**, *150*, A1246−A1249.
(49) Izawa, H.; Kikkawa, S.; Kolzum, M. *J. Phys. Chem.* **1982**, *86*, 5023−5026.

clinic" TiO_2 reported in ref 47 seems to be identical to TiO_2(B)).

Li et al.[48] have recently reported on the lithium insertion into hydrothermally grown TiO_2 nanotubes. The material showed good capacity and cycle life. Its cyclic voltammogram exhibited some features of organized mesoporous anatase made by surfactant templating,[4,20] but this analogy was not commented on in ref 48. The present paper aims at addressing these issues by a systematic study of lithium insertion into titania nanostructures made by hydrothermal growth in NaOH medium. There is a challenge that the rich structural chemistry of hydrothermally grown titania nanostructures may be mirrored also in their electrochemical properties.

Experimental Section

Materials. Thirty-four research samples were obtained from SusTech GmbH & Co. KG, Darmstadt, Germany. Their general synthetic protocol was as follows: 8 mL (72.9 mmol) of $TiCl_4$ was dissolved in 20 mL of water. Then, 10 N NaOH was added to a total volume of 150 mL. The mixture was autoclaved at 250 °C for 6 h. Subsequently, the material was washed with hydrochloric acid and water and further autoclaved in water or weak acidic solvents for up to several hours. The individual samples are listed in the Supporting Information along with their basic properties (BET surface areas and phase composition). The concentration of anatase phase was determined from powder X-ray diffraction according to a method developed by Banfield et al.[50] Rutile (Bayer R-U-F, containing 3.7 wt % anatase) served as an inner reference in the phase analysis. Nanocrystalline anatase Bayer PKP09040 (154 m^2/g as-received; 89 m^2/g after sintering into a thin-film electrode)[3] was used as another reference material, and it further served for comparative experiments with *n*-butyllithium (vide infra). Still another reference material (C240, 89 m^2/g after sintering into a thin-film electrode) was made by the sol−gel method and autoclaved in water at 240 °C. (Both Bayer PKP09040 and C240 are pure anatase nanocrystals with ordinary grain morphology (see ref 3 for details)).

Preparation of Electrodes. A powder sample was dispersed in an aqueous medium into a viscous paste according to the previously developed methods.[3,51,52] The powder (0.3 g) was mixed under stirring or gentle mortaring with 0.8 mL of 10% aqueous solution of acetylacetone. Subsequently, 0.8 mL of 4% aqueous solution of hydroxypropylcellulose (Aldrich, MW 100 000) was added and finally 0.4 mL of 10% aqueous solution of Triton-X100 (Fluka). Before use, the prepared slurry was homogenized by stirring. If the slurry was too viscous, it was further diluted by water. Titanium grid (5 × 15 mm, Goodfellow) was used as the electrode support. Electrodes were prepared by dipcoating; the coated area was ca. 5 × 5 mm. The prepared electrodes were dried in air and finally calcined in air at 450 °C for 30 min. The amount of active electrode material was between 0.2 and 0.7 mg. Blank experiments confirmed that a bare Ti grid had negligible electrochemical charge capacity compared to that of the active material. Alternatively, the slurry was also deposited on a sheet of conducting glass (F-doped SnO_2, TEC 8 from Libbey-Owens-Ford, 8 Ω/square) using a doctor-blading technique.[3,53] The sheet of conducting glass had the dimensions 3 × 5 × 0.3 cm^3. Scotch tape at both edges of the support (0.5 cm) defined the film thickness and left part of the support uncovered for electrical contact. The film was finally calcined for 30 min in air at 450 °C. After cooling to room temperature, the sheet was cut into 10 electrodes, 1.5 × 1 cm^2 in size; the geometric area of the TiO_2 film was 1 × 1 cm^2. Sometimes the TiO_2 layers on conducting glass were mechanically unstable and delaminated easily from the support after electrochemical treatment. The layers deposited on a Ti grid were satisfactorily stable.

Methods. Electrochemical measurements were carried out in a one-compartment cell using an Autolab Pgstat-30 (Ecochemie) controlled by the GPES-4 software. The reference and auxiliary electrodes were from Li metal; hence, potentials are referred to the Li/Li^+ (1 M) reference electrode. $LiN(CF_3SO_2)_2$ (Fluorad HQ 115 from 3M) was dried at 130 °C/1 mPa. Ethylene carbonate (EC) and 1,2-dimethoxyethane (DME) were dried over the 4A molecular sieve (Union Carbide). The electrolyte solution, 1 M $LiN(CF_3SO_2)_2$ + EC/DME (1/1 by volume) contained 15−40 ppm H_2O as determined by Karl−Fischer titration (Metrohm 684 coulometer). All operations were carried out under argon in a glovebox. Transmission electron microscopy (TEM) images were obtained on a Tecnai F30 microscope with a 300-keV field emission electron gun. The BET surface areas of the prepared materials were determined from nitrogen adsorption isotherms at 77 K (ASAP 2010, Micromeritics). Powder X-ray diffraction (XRD) was studied on a Siemens D-5000 diffractometer using Cu Kα radiation. Samples treated by *n*-butyllithium (10 min of stirring in 1.6 M solution in hexane (Aldrich) with a molar ratio Li/Ti ∼ 2) were washed with hexane and dried under Ar. The airtight sample container covered by Kapton foil was used for recording XRD patterns.[15] Raman spectra were excited by an Ar^+ laser at 2.54 eV (Innova 305, Coherent) and recorded on a T-64000 spectrometer (Instruments, SA) interfaced to an Olympus BH2 microscope (objective 50×). Microscopic measurements allowed focusing on different sampled areas (different grains of the solid material) to test the homogeneity of studied samples.

Results and Discussion

Figure 1 shows a typical morphology of the prepared samples. The materials contain nanoribbons or elongated nanosheets, which may be curved and partly or fully rolled into tubes.[32,35,36,38−40] The rolling is visualized on the high-resolution image, along with the fringes parallel to the ribbon axis. This morphology is reminiscent of that reported by Su et al.[40]

The phase analysis according to Banfield[50] (see Experimental Section) usually indicated a low content of crystalline TiO_2 in most materials tested. Phenomenologically, this indicates the presence of some "X-ray amorphous" (XRA) phase. The term XRA refers to material, which does not exhibit distinct diffraction peaks, but which may still possess low-range ordering. Hence, it might well be the titania nanosheet, nanotube, or simply a nanocrystal, which is too small to be detectable by powder XRD. (Note that the pristine exfoliated nanosheets of the lepidocrocite-like titania are also virtually "X-ray amorphous",[44−46] but electron diffraction indicates their two-dimensional face-centered orthogonal arrangement.[54]) The actual XRA concentrations of all tested materials are quoted in the Supporting Information.

According to XRD, all the tested materials contained anatase as the main phase. The materials Lor-035-092A (67 m^2/g, XRA = 80%) and Lor-035-013B (18 m^2/g, XRA >95%) exhibited some features at 2Θ ∼ 10° (Cu Kα),

(50) Zhang, H.; Finnegan, M.; Banfield, J. F. *Nano Lett.* **2001**, *1*, 81−85.
(51) Kavan, L.; O'Regan, B.; Kay, A.; Grätzel, M. *J. Electroanal. Chem.* **1993**, *346*, 291−307.
(52) Nazeeruddin, M. K.; Kay, A.; Rodicio, I.; Humphry-Baker, R.; Mueller, E.; Liska, P.; Vlachopolous, N.; Grätzel, M. *J. Am. Chem. Soc.* **1993**, *115*, 6382−6390.
(53) Burnside, S. D.; Moser, J.; Brooks, K.; Grätzel, M.; Cahen, D. *J. Phys. Chem. B* **1999**, *103*, 9328−9332.
(54) Sasaki, T.; Ebina, T.; Kitami, Y.; Watanabe, M. *J. Phys. Chem. B* **2001**, *105*, 6116−6121.

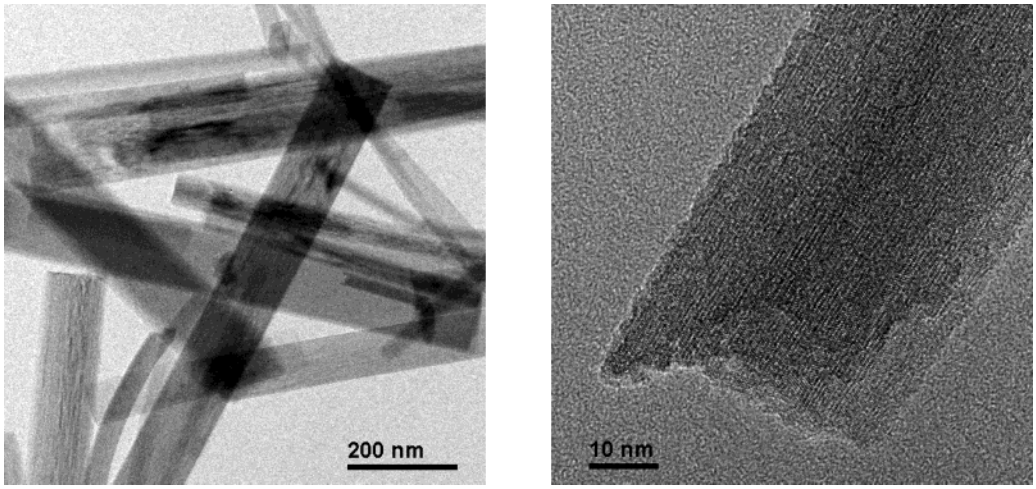

Figure 1. TEM picture demonstrating a typical morphology of the SusTech materials (sample Lor-035-013B, XRA>95%; see Supporting Information for further details).

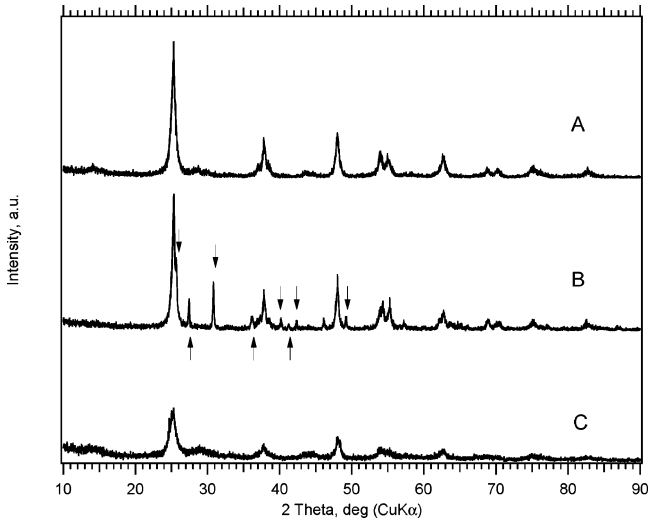

Figure 2. X-ray diffraction pattern of selected SusTech materials: [A] sample Lor-035-088C (XRA = 17%), [B] sample Lor-035-099A (XRA = 48%), and [C] sample Lor-035-092D (XRA = 56%). The plot [B] evidences the presence of anatase, rutile (upward-directing arrows), and brookite (downward-directing arrows).

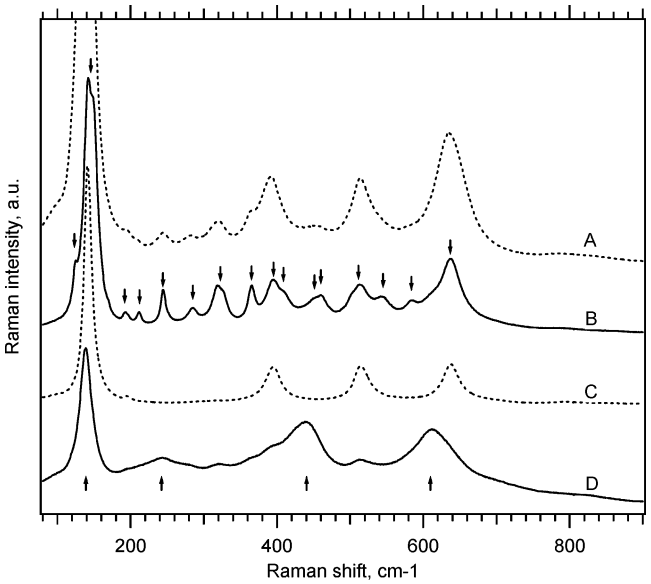

Figure 3. Micro-Raman spectra of selected SusTech materials: [A] Lor-035-112B2 (XRA = 32%), [B] Lor-035-099A (XRA = 48%), [C] Lor-035-098c (XRA <1%) spectrum assignable to pure anatase, and [D] Lor-035-112B2 different sample area (cf. plot [A]). Downward-directing arrows, brookite; upward-directing arrows, rutile.

which is a diagnostic diffraction for the layered protonic titanates. Most other materials exhibited only weak- or negligible peaks in this region. In several cases also rutile and brookite impurities were found. This is demonstrated in Figure 2 on the diffractogram of sample Lor-035-099A (53 m^2/g, XRA = 48%), which can be indexed as a mixture of anatase, rutile, and brookite.

Further insight into the phase composition of the SusTech materials can be obtained from micro-Raman spectroscopy. This technique allows selecting a sampled area of several micrometers in size, and by scanning of the sample surface, we can distinguish different Raman-active phases in a sample. Figure 3 displays illustrative examples of mixed-phase (plots A, B, D) and pure-phase (plot C) materials. The latter plot evidences a pure anatase phase in Lor-035-098c (XRA <1%), in accord with X-ray diffraction. Most other SusTech materials exhibited pure anatase also by the Raman tests (see Supporting Information). However, plots B and D demonstrate that, with the mentioned spatial resolution, we can, sometimes, find sampled micro-areas corresponding to brookite[55] and rutile, respectively. Spectrum A is an example of an anatase + brookite mixture seen in one position on the sample Lor-035-112B2 (XRA = 32%), but we can also focus to another area in the same material, exhibiting mostly the rutile phase. Several samples from the tested set of materials contained all three main phases of TiO_2, that is, anatase, rutile, and brookite, while we can find a "Raman-pure" phase in the sampled area of several micrometers in size.

Figure 4 shows an example of a cyclic voltammogram at the conditions of Li^+ insertion into the material Lor-035-071A (135 m^2/g, XRA = 71%; pure anatase seen by XRD and Raman). This voltammogram exhibits an unusual shape, if we compare it to the voltammograms

(55) Tompsett, G. A.; Bowmaker, G. A.; Cooney, R. P.; Metson, J. B.; Rodgers, K. A.; Seakins, J. M. *J. Raman Spectrosc.* **1995**, *26*, 57−62.

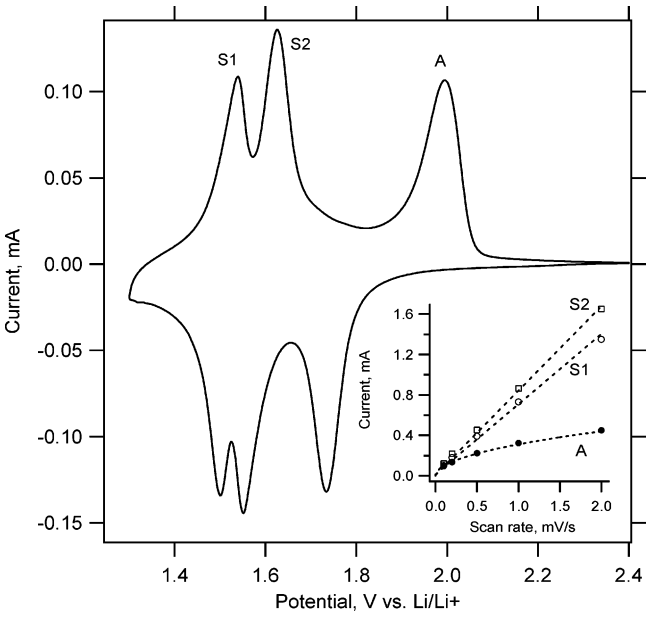

Figure 4. Cyclic voltammograms of the material Lor-035-071A (135 m^2/g, XRA = 71%; pure anatase seen by XRD and Raman). Electrolyte solution: 1 M $LiN(CF_3SO_2)_2$ + EC/DME (1:1, v:v); scan rate 0.1 mV/s. Inset: anodic peak current vs the scan rate.

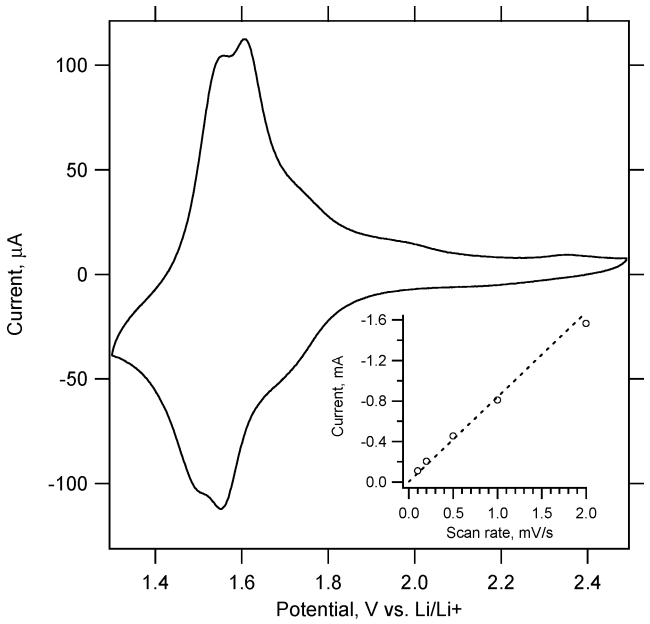

Figure 5. Cyclic voltammograms of the material Lor-035-013B (calcined for 7 h at 400 °C, XRA > 95%). Electrolyte solution: 1 M $LiN(CF_3SO_2)_2$ + EC/DME (1:1, v:v); scan rate 0.1 mV/s. Inset: cathodic peak current vs the scan rate.

of "ordinary" anatase, both in the form of single crystal[8,9] or nonorganized nanocrystalline[1−4,13] electrodes. The voltammogram is dominated by two pairs of peaks denoted S1 and S2. The formal potentials of S1 and S2 peaks are 1.52 and 1.59 V vs Li/Li^+, respectively. The remaining pair of peaks (formal potential 1.88 V; denoted A) is commonly observed in anatase electrodes.[1−4,8,9,13] The same effect was previously reported only in the mesoporous anatase films made by supramolecular templating with Pluronic.[20] In this case, the extra peaks (S-peaks) were tentatively assigned to the presence of "amorphous titania".[20]

Inserted in Figure 4 is a plot of the peak current vs scan rate. The peak current ($I_{p,A}$) of A-peaks scales with the square root of the scan rate, v, as is expected for diffusion-controlled irreversible kinetics,[1,12]

$$|I_{p,A}| = 0.4958nFAc(D\alpha nFv/RT)^{1/2} \qquad (2)$$

where n is the number of electrons, A is the electrode area, c is the maximum concentration of Li^+ (or Ti^{3+}) in the accumulation layer (c = 0.024 mol/cm^3 for x = 0.5; cf. eq 1), D is the chemical diffusion coefficient of Li^+, and the other symbols have their usual meaning.

On the other hand, the peak currents of S1/S2 peaks ($I_{p,S}$) scale with the first power of the scan rate, which is characteristic for capacitive charging:

$$|I_{p,S}| = A\ dQ/dt = AC\ dE/dt = ACv \qquad (3)$$

Q is the voltammetric charge and dE/dt the scan rate, v. However, the characteristic shape of the voltammogram with small peak-to-peak splitting (ca. 50−100 mV at v = 0.1 mV/s) points at some surface-confined faradaic process.

The capacitive and/or surface-confined faradaic process is developed explicitly on materials which are rich in XRA phase. Figure 5 shows an example material, which has almost no A-peaks, but a broad feature in the area of S1/S2 peaks. This is reminiscent of the behavior of "amorphous" titania made by anodic oxidative hydrolysis of $TiCl_3$.[20]

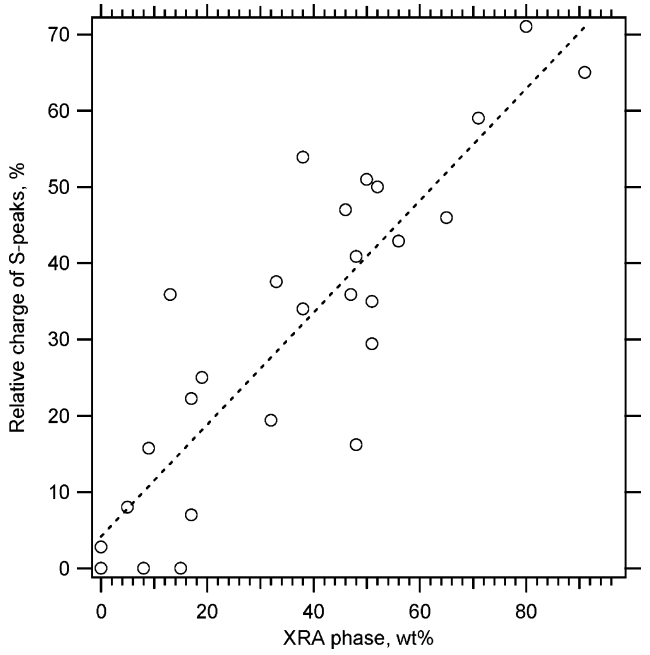

Figure 6. Integral voltammetric charge of the S-peaks (S1 + S2; referred to the total charge) from the anodic branch of cyclic voltammograms (scan rate 0.2 mV/s) is plotted as a function of the concentration of "X-ray amorphous" (XRA) phase in the material. The dashed line is a linear fit of experimental points.

Twenty-six different materials from the tested set of samples exhibited well-developed S-peaks. Their formal potentials (1.52 and 1.59 V) were reproducible with a deviation smaller than ±0.01 V for all the "S-active" samples. The area (charge) of S-peaks was variable, but it correlated with the content of XRA phase in the particular material. Figure 6 displays the proportion of integral voltammetric charge of the S1/S2 peaks (re-

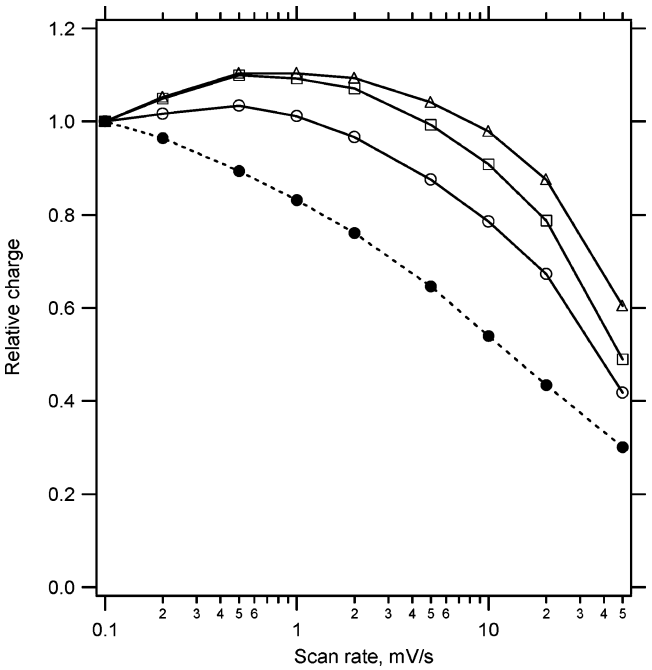

Figure 7. Integral voltammetric charge from the anodic branch of cyclic voltammograms (as in Figures 4, 5) is plotted as a function of scan rate. The charge was normalized against the charge capacity of the same electrode at the slowest scan (0.1 mV/s). Open points, material Lor-035-119A (85 m^2/g XRA = 19%); squares, material Lor-035-119B (43 m^2/g, XRA = 38%); triangles, material Lor-035-071a (135 m^2/g, XRA = 71%). Full points + dashed line, reference nonorganized nanocrystalline anatase C240 (89 m^2/g, XRA ≅ 0).

ferred to the total charge capacity) as a function of the concentration of XRA phase. This correlation matches the heuristic conclusion of ref 20 that the S-peaks are signatures of "amorphous titania" in the sample. The explicit advantages of hydrothermally grown TiO_2 nanostructures over the Pluronic-templated materials[20] consist of (i) broad selection of materials with varying proportion of XRA phase and (ii) their availability as powders in macroscopic quantity. This allows investigation of this peculiar effect in detail.

Figure 7 plots the total voltammetric charge of the material Lor-035-071a (anatase, XRA = 71%; 135 m^2/g) against the scan rate. For comparison, the same curve is plotted for two other similar SusTech samples and compared to that of nonorganized nanocrystalline anatase (C240, 89 m^2/g) made by sol−gel.[3] As the absolute charge capacities of each testing electrode fluctuated (between ca. 150 and 400 mC), the data in Figure 7 were normalized with respect to the actual charge of the same electrode at the slowest scan (0.1 mV/s) which was set as unity. Figure 7 demonstrates that the SusTech materials delivered the reference charge already at ca. 1−5 mV/s, while there seems to be even some unexpected increase above one at medium scan rates (0.2−1 mV/s). The same peculiarity in $Q-v$ plots was observed also for the Pluronic-templated materials,[20] and this study has confirmed that such a behavior is another characteristic feature of materials exhibiting S-peaks. Ordinary nonorganized nanocrystalline anatase shows the "normal" monotonic increase of voltammetric charge with decreasing scan rate (cf. also refs 3 and 20).

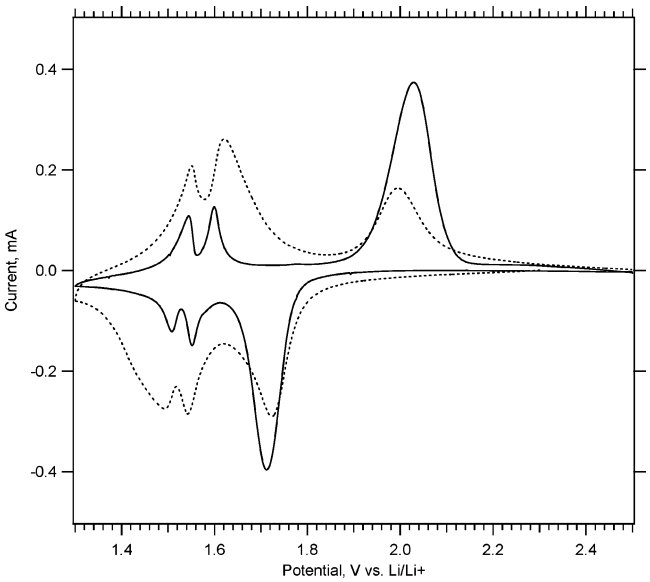

Figure 8. (Dashed line): Cyclic voltammogram of material Lor-035-094b (XRA = 91%). (Full line): The same material after heat treatment for 40 h at 500 °C. The absolute currents are not comparable since the plots represent two different electrodes. Electrolyte solution: 1 M $LiN(CF_3SO_2)_2$ + EC/DME (1:1, v:v); scan rate 0.2 mV/s.

The voltammetric charge in ordinary anatase corresponds to the A-peaks only, and the process is controlled by a diffusion of Li^+ in the solid (eq 2). On the other hand, the materials with S-peaks show a pronounced charge, which is assigned to a surface-confined charge transport. This process mimics the fast capacitive charging (eq 3). The analogy goes further, as the capacitive charging is also more sensitive to self-discharge, as for any supercapacitor. This may explain the appearance of a maximum in the $Q-v$ plot shown in Figure 7. The charging in S-peaks should not be confused with the ordinary double-layer charging, which is inherently free from any peaks (cf. also ref 20). We suggest that the charge of S-peaks can be considered as a faradaic pseudocapacitance, specific for certain materials containing the XRA phase (vide infra).

The absolute faradaic capacity of our materials cannot be measured very precisely, owing to the small mass of active electrode material (see Experimental Section). Nevertheless, there was a clear trend for increasing the Li-charge capacity with increasing S-peak area (XRA content). For slow voltammetric charging ($v \sim 0.1$ mV/s) the materials without S-peaks (XRA → 0) exhibited a reversible charge capacity of about 600 C/g, which is a typical value for anatase electrodes (with A-peaks only).[1−4] The "S-active" materials exhibited significantly larger capacities, up to ca. 800 C/g. A similar enhancement of the capacity of hydrothermally grown TiO_2 nanotubes was reported by Li et al.[48] Obviously, the S-peaks increase the Li-storage capacity, due to a more favorable stoichiometry, accessible in the pseudocapacitive process (vide infra).

The S-peaks in Pluronic-templated materials were found to be completely quenched by long-term (40 h) heat treatment at 450 °C.[20] Our nanostructures showed similar tendency, although their thermal stability was higher. This is illustrated by the behavior of one example material in Figure 8. The heat treatment of

this material at 500 °C for 40 h does not cause a complete disappearance of S-peaks, but only decreases their intensity. The analogy of our materials with Pluronic-templated ones[20] manifests itself also by larger A-peaks splitting in annealed materials. We recall an empirical correlation showing that the splitting of A-peaks is linearly proportional to the particle size of anatase.[4] This confirms the hypothesis that the anatase crystals grow upon heat treatment from the XRA phase.

The nature of S-peaks is still not yet fully understood. They occur specifically in Li^+-containing electrolyte solutions; that is, they are not produced by larger cations, such as K^+.[20] Phenomenologically, their incidence correlates with the presence of "amorphous" titania, both in Pluronic-templated materials[20] and in the hydrothermally grown nanostructures, presented here (cf. Figure 6). On the other hand, the perfect reproducibility of the position of S-peaks (among a wide selection of materials, including the Pluronic-templated ones[20]) points at a process involving well-defined structural conditions. This is difficult to reconcile with the presence of a poorly defined "amorphous" titania. S-peaks rather indicate a distinguished nanophase whose structure is regular and defined, albeit not X-ray detectable. (Note that the "truly amorphous" titania does not show the S-peaks, but just a broad envelope of features at similar potentials.[20])

On the basis of the data collected in this work, we propose that the S-peaks are caused by the interaction of Li^+ ions with titania nanosheets. The nanosheets are formed via exfoliation of layered protonic titanates, and during calcination, they are converted to a nonstoichiometric TiO_2, preserving the sheet morphology. The nanosheets may even show the anatase-like ordering, oriented along the *c*-axis.[39,40] Analogously, the calcination of lepidocrocite-like titania leads to anatase-like sheets oriented along the *c*-axis.[56] The parent protonic titanates, such as $H_2Ti_3O_7$ and $H_2Ti_4O_9$, are semiconductors, whose band gap energy is larger by ca. 0.1 eV compared to that of anatase.[57] (Note, however, a reference for the opposite statement, too.[41]) Also the lepidocrocite-like titania shows slightly larger band gap energy (3.24 eV), which increases however significantly upon exfoliation into individual nanosheets.[46,58] Recent theoretical calculations further confirmed that such a two-dimensional titania shows larger band gap energy than anatase.[59]

The increase of band gap energy, ΔE_g in ultrasmall crystallites[60] or ultrathin layers[58,59] of TiO_2, has been attributed to the quantum-size effect:

$$\Delta E_g = \frac{h^2}{8\mu_{xy}}\left(\frac{1}{L_x^2} + \frac{1}{L_y^2}\right) + \frac{h^2}{8\mu_z L_z^2} \qquad (4)$$

where h is the Planck constant, μ designates the reduced effective masses of the excitons, and L corresponds to the crystal dimension. The subscripts x and y denote coordinates parallel to the layer, and z is perpendicular to the layer. Since $L_z \ll L_x, L_y$, the first term in eq 4 can be neglected for a nanosheet. The blue shift of ΔE_g in ca. 1−2-nm-sized anatase crystals is accompanied by a negative shift of the flatband potential by ca. 0.2 V.[60] We may note that the cathodic S-peaks are negatively shifted by nearly the same potential difference compared to the cathodic A-peak (Figure 4). Consequently, the nanosheets are idle at the potential of Li^+ insertion into anatase, and they start to accommodate Li^+ only below their flatband potential. We may even rationalize why the S-peaks occur in two pairs, if we accept the notion that the nanosheets have (101) or (001) orientations[40] and that the different faces of anatase can have different flatband potentials.[8] In fact, we have shown that the flatband potentials of (101) and (001) faces differ by 0.06 V and the ability of accommodating Li^+ is also different.[8] (Note that the separation of S-peak is 0.07 V, which is close to the mentioned separation for the two anatase faces.) The nature of Li^+/nanosheet interaction is unknown, but we may note that a nanosheet composed from edge-sharing TiO_6 octahedra[35,42−44,54,58,61] contains two types of oxygen atoms: those which are shared by the neighboring octahedra and those which belong to a single octahedron on the topmost position on the surface (Scheme 1). These topmost oxygens are ca. 0.15 nm above the surface layer composed of Ti atoms and shared oxygens.[45]

Scheme 1. Cross-sectional View on the Titania Nanosheet Composed from Edge-Sharing TiO_6 Octahedra[a]

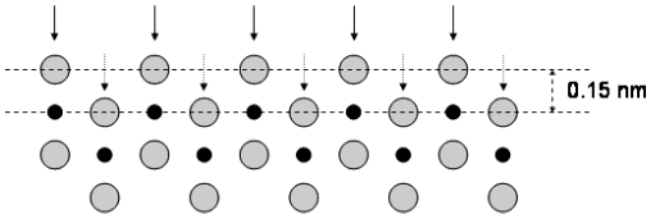

[a] The oxygen atoms at the topmost corner positions are marked by full arrows and oxygen atoms at the edge-sharing positions are marked by dashed arrows. The small full points stand for Ti atoms.

It is tempting to suggest that these two oxygen sites are responsible for the double-peak structure of S-peaks. Recently, Wagemaker et al.[19] have demonstrated two distinct positions in a network of TiO_6 octahedra, where Li may be accommodated. This provides another rational for the doublet structure of the S-peaks.

The pseudocapacitive behavior of S-peaks is readily explained in terms of the interaction taking place on the nanosheet surface. The nanosheet is composed of just two planes of edge-sharing TiO_6 octahedra (cf. Scheme 1), which are either kinked (monoclinic structures) or perfectly flat (lepidocrocite-like structures).[35,42−45,49,57,58,61] Hence, the compensation of electronic charge, injected into the conduction band, does not require any solid-state transport of Li^+ cations. This hypothesis may apply both for the flat nanosheets as well as for the curved ones, and, eventually, for the nanotubes with spiral-like rolling. These structures are

(56) Fukuda, K.; Sasaki, T.; Watanabe, T.; Nakai, I.; Inaba, K.; Omote, K. *Cryst. Growth Des.* **2003**, *3*, 281−283.
(57) Kim, Y. I.; Atherton, S. J.; Brigham, E. S.; Mallouk, T. E. *J. Phys. Chem.* **1993**, *97*, 11802−11810.
(58) Sasaki, T.; Watanabe, M. *J. Phys. Chem. B* **1997**, *101*, 10159−10161.
(59) Sato, H.; Ono, K.; Sasaki, T.; Yamagishi, A. *J. Phys. Chem. B* **2003**, *107*, 9824−9828.
(60) Kavan, L.; Stoto, T.; Grätzel, M.; Fitzmaurice, D.; Shklover, V. *J. Phys. Chem.* **1993**, *97*, 9493−9498.
(61) Sasaki, T.; Watanabe, M.; Michiue, Z.; Komatsu, Z.; Izumi, F.; Takenouchi, S. *Chem. Mater.* **1995**, *7*, 1001−1007.

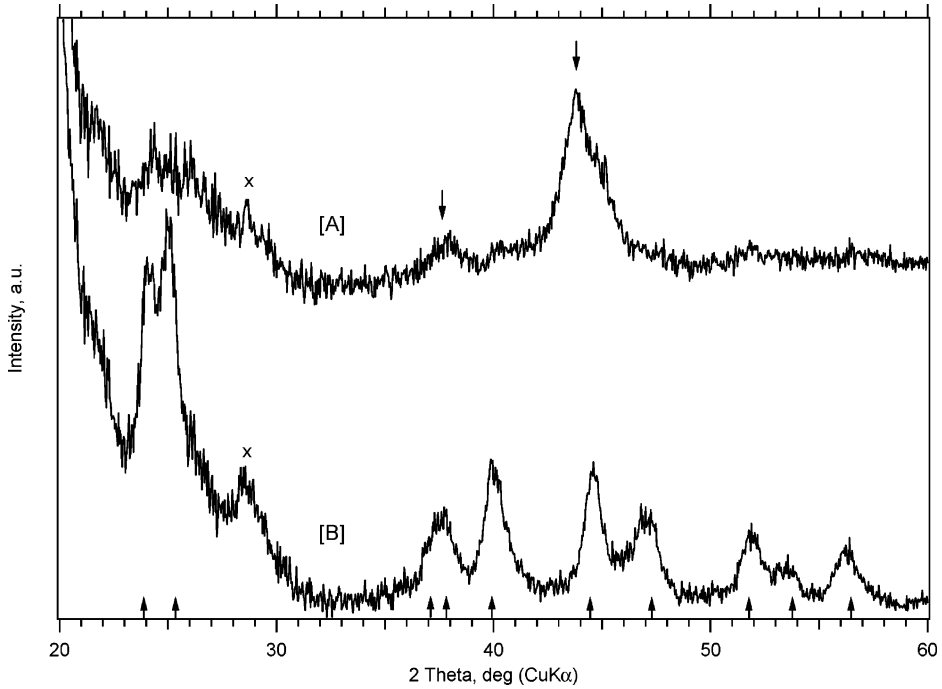

Figure 9. X-ray diffraction pattern of materials after reaction with *n*-butyllithium: [A] sample Lor-035-094b (150 m^2/g, XRA = 91%, anatase only seen by XRD and Raman); [B] nanocrystalline anatase Bayer PKP09040 (154 m^2/g, XRA ≅ 0, anatase only seen by XRD and Raman). The signal of Kapton foil is marked by ×. The diffraction lines of orthorhombic $Li_{0.5}TiO_2$ are marked by upward-directing arrows and the lines of cubic $LiTiO_2$ are marked by downward-directing arrows.

open; hence, their surface is accessible for electrochemical reactions. This raises the question whether similar nanosheets occur also in the Pluronic-templated materials (exhibiting S-peaks),[20] despite explicit differences in the synthetic protocol of these materials.[20,62−65] The Pluronic-templated TiO_2 contains, reportedly, anatase nanocrystals embedded in "amorphous" titania, whose structure was not specified.[20,62−65] The assembly is mesoporous with either a 2-D hexagonal (*p*6*m*) or a 3-D cubic (*Im*3*m*) arrangement.[63] However, Stucky et al.[65] have recently reported an additional structure designated as *lamellar titania*, which may grow in Pluronic-templated materials at larger concentrations of Pluronic polymer. It appears therefore that the S-peaks observed in ref 20 with the Pluronic-templated materials arise from a lamellar form of titania and not an amorphous one as originally suggested by us.[20] The present study clearly shows that the appearance of the characteristic feature of the S-double peaks in the cyclic voltammogram can be used as a diagnostic tool for the presence of such sheetlike titania nanostructures.

The specific nature of our materials is also demonstrated by their chemical reaction with *n*-butyllithium. This reagent is known to mimic the electrochemical Li insertion, corresponding to a potential of ca. 1 V vs Li/Li^+ electrode.[15] Figure 9 shows that the ordinary nanocrystalline anatase (Bayer PKP09040) is converted to an orthorhombic lithium titanate $Li_{0.5}TiO_2$, in agreement with previously published data.[13,15] (A quantitative conversion into this sole product was traced even for the ratio Li/Ti = 0.7.[15]) At the same conditions, our materials with high XRA content produce upon chemical lithiation another phase, which can be indexed as cubic lithium titanate $LiTiO_2$.

We have usually observed mixtures of both phases (orthorhombic and cubic) after the treatment with *n*-butyllithium. However, the materials exhibiting large S-peaks (large XRA content) showed also larger proportion of the cubic titanate. An explicit example is the material Lor-035-094b (150 m^2/g, XRA = 91%, anatase only seen by XRD and Raman), which gave almost pure cubic lithium titanate $LiTiO_2$ after the reaction with *n*-butyllithium (Figure 9). Apparently, the nanosheets are easily accessible to chemical reduction, yielding a Li-rich product under the conditions, when bulk anatase gives only the orthorhombic lithium titanate $Li_{0.5}TiO_2$. Note that this conclusion agrees with the electrochemically determined Li-storage capacities, exceeding 600 C/g ($x \cong 0.5$), vide ultra.

In summary, TiO_2 exhibiting S-peaks is a promising charge storage material. It accommodates Li^+ by three different mechanisms: (1) Li insertion into the anatase lattice (with subsequent reversible conversion to orthorhombic titanate), (2) double-layer charging, and (3) the surface-confined charge storage specific for certain "amorphous" titania, which was identified here as interaction with titania nanosheets. While the mechanisms (1, 2) are ubiquitous in all Li-insertion hosts, the mechanism (3) is a specific property of special TiO_2 materials only. The double-layer charging (effect 2) is omnipresent at all potentials below the flatband potential. On the other hand, the effects (1) and (3) occur at well-distinguished potentials. This offers another spe-

(62) Yang, P.; Zhao, D.; Margolese, D. I.; Chmelka, B. F.; Stucky, G. D. *Chem. Mater.* **1999**, *11*, 2813−2826.
(63) Crepaldi, E. L.; Soler-Illia, G. J. A. A.; Grosso, D.; Cagnol, F.; Ribot, F.; Sanchez, C. *J. Am. Chem. Soc.* **2003**, *125*, 9770−9786.
(64) Yang, P.; Zhao, D.; Margolese, D. I.; Chmelka, B. F.; Stucky, G. D. *Nature* **1998**, *396*, 152−155.
(65) Alberius, P. C. A.; Frindell, K. L.; Hayward, R. C.; Kramer, E. J.; Stucky, G. D.; Chmelka, B. F. *Chem. Mater.* **2002**, *14*, 3284−3294.

cific application of our materials: Depending on the applied potential window, the material behaves either as a Li-insertion host (between ca. 1.7 and 2.1 V) or as a pure supercapacitor (between ca. 1.3 and 1.7 V). Figures 4 and 6 evidence that the ratio of charge of supercapacitor/Li insertion can vary in a broad range from 0 to ca. 2.3. These two different charging regimes may find application in special energy storage devices. Larger Li-storage capacity, up to ca. 800 C/g, and faster kinetics of Li charging are other explicit advantages of these materials.

Acknowledgment. This work was supported by NTera Ltd., the Swiss CTI Top Nano-21 program (Contract No. 5775.1), the EC-COST Action D14/0002/99, and the Grant Agency of the Czech Republic (Contract No. 203/03/0824). We are grateful to Prof. Joop Schoonman (Delft University of Technology) for reading the manuscript and helpful comments.

Supporting Information Available: Survey of the tested SusTech materials (PDF). This material is available free of charge via the Internet at http://pubs.acs.org.

CM035046G